Diagnosing Fractionalization from the Spin Dynamics of Z_2 Spin Liquids on the Kagome Lattice by Quantum Monte Carlo Simulations

Jonas Becker and Stefan Wessel
Institut für Theoretische Festkörperphysik, JARA-FIT and JARA-HPC, RWTH Aachen University, 52056 Aachen, Germany

(Received 5 April 2018; published 14 August 2018)

Based on large-scale quantum Monte Carlo simulations, we examine the dynamical spin structure factor of the Balents-Fisher-Girvin kagome lattice spin-1/2 model, which is known to harbor an extended Z_2 quantum spin liquid phase. We use a correlation-matrix sampling scheme combined with a stochastic analytic continuation method to resolve the spectral functions of this anisotropic quantum spin model with a three-site unit cell. Based on this approach, we monitor the spin dynamics throughout the phase diagram of this model, from the XY-ferromagnetic region to the Z_2 quantum spin liquid regime. In the latter phase, we identify a gapped two-spinon continuum in the transverse scattering channel, which is faithfully modeled by an effective spinon tight-binding model. Within the longitudinal channel, we identify gapped vison excitations and exhibit indications for the translational symmetry fractionalization of the visons via an enhanced spectral periodicity.

DOI: 10.1103/PhysRevLett.121.077202

The search for quantum spin liquid (QSL) states in frustrated magnets remains an active area of research in condensed matter physics [1–3]. As topologically ordered states of matter [4], gapped QSLs exhibit long-ranged many-body entanglement and fractionalized excitations beyond one dimension. In order to identify QSL states in actual materials, spectroscopic measurements such as inelastic neutron scattering constitute valuable diagnostic tools, e.g., by detecting scattering continua due to deconfined fractionalized spin excitations or anyonic statistics [5]. Thus, it is important to obtain unbiased theoretical predictions for the corresponding dynamical spin structure factor (DSSF) of fundamental microscopic models with gapped QSL phases. A hallmark two-dimensional geometry in support of strong geometric frustration is the kagome lattice of corner-sharing triangles. An unbiased theoretical characterization of kagome-lattice based QSL phases in terms of spectroscopic probes is important in view of the compound $ZnCu_3(OH)_6Cl_2$ (herbertsmithite) [6,7], as well as $Cu_3Zn(OH)_6FBr$ (Zn-doped barlowite), put forward recently as a possible spin-1/2 kagome gapped QSL candidate [8–10]. While indications of a gapped QSL ground state in the antiferromagnetic Heisenberg model on the kagome lattice have been reported [11–14], other recent numerical results indicate that, instead, a gapless QSL may be realized in this model [15–18]. This leaves the stability of a gapped topological QSL open for this fundamental SU(2)-symmetric model of kagome-lattice based quantum spin physics.

In this respect, it is comforting that another, though anisotropic, spin-1/2 model by Balents, Fisher, and Girvin (BFG) has been established to harbor an extended gapped QSL on the kagome lattice [19], characterized as a Z_2 topologically ordered state [20,21]. As such, this model hosts gapped deconfined spinons, i.e., spin-1/2 excitations, in sharp contrast to conventional integer spin excitations such as magnons. In terms of anyonic statistics, the spinons in the BFG model are bosonic [19]. In addition, the topological QSL phase of the BFG model also exhibits gapped vortex excitations of an emerging odd-structured Ising gauge field [22–24], the so-called "visons" [25–27]. Within a resonating valence bond (RVB) description of the QSL ground state, a single vison excitation effects sign changes in the RVB superposition of singlet states across a semi-infinite line [19]. Carrying neither charge nor spin, visons do not couple directly to neutrons but can be probed through their interaction with spinons [28]. Furthermore, their existence leads to a topology protected fourfold ground state degeneracy in a system with periodic boundary conditions in both lattice directions [19–21]. The BFG model, along with several variants, was, indeed, shown to exhibit a topological contribution to the ground state entanglement as well as symmetry-protected edge states due to nontrivial symmetry fractionalization [29–34]. Part of this progress was possible since this model allows for sign-problem free, unbiased quantum Monte Carlo (QMC) simulations on relatively large lattices. Hence, the BFG model is well suited for probing the spin dynamics of Z_2 QSL states on the kagome lattice for gapped deconfined spinon and vison excitations, based on unbiased QMC simulations.

Thus, here, we consider this basic model of an extended Z_2 QSL phase on the kagome lattice to study the corresponding DSSF using advanced QMC methods. We identify characteristic features of fractionalization in the QSL phase and contrast them to the DSSF in the XY-ferromagnetically

ordered region of this model. The Hamiltonian that we consider reads [cf. Fig. 1(a)] $H = -J\sum_{\langle j,j'\rangle}(S_j^+ S_{j'}^- + S_j^- S_{j'}^+) + (J_z/2)\sum_{\hexagon}(S_{\hexagon}^z)^2$, in terms of a ferromagnetic ($J > 0$) nearest neighbor transverse spin exchange and longitudinal antiferromagnetic interactions of strength $J_z > 0$ on all bonds within the hexagons of the kagome lattice, compactly expressed in terms of the hexagonal cluster terms, $S_{\hexagon}^z = \sum_{j\in\hexagon} S_j^z$. In the following, we consider finite rhombic systems with $N_s = 3L^2$ lattice sites and periodic boundary conditions along both lattice directions $\mathbf{a}_1$, $\mathbf{a}_2$ in Fig. 1(a), with the unit cell distance fixed to $a = 1$. The first Brillioun zone (BZ), in terms of the reciprocal lattice vectors $\mathbf{b}_1$, $\mathbf{b}_2$, is shown in Fig. 1(b). The Hamiltonian H was shown in previous studies to harbor a QSL ground state for small values of J that is separated from an XY-ferromagnetic region by a quantum critical point at $J/J_z = 0.07076(1)$, which was identified as an XY^* transition [32,33], cf. Fig. 1(c). To formulate the DSSF of the three-sublattice kagome lattice, we denote by $\mathbf{S}_{i,\alpha}$ the spin at position $\mathbf{r}_{i,\alpha}$ on sublattice α (= 1, 2, 3) in the ith unit cell ($i = 1, \ldots, L^2$), and then obtain 3×3 correlation-matrices $S^{+-}_{\alpha,\beta}(\mathbf{k},\omega) = \int dt e^{-i\omega t}\langle S^+_{\mathbf{k},\alpha}(t)S^-_{-\mathbf{k},\beta}(0) + S^-_{\mathbf{k},\alpha}(t)S^+_{-\mathbf{k},\beta}(0)\rangle$ for the transverse, and $S^{zz}_{\alpha,\beta}(\mathbf{k},\omega) = \int dt e^{-i\omega t}\langle S^z_{\mathbf{k},\alpha}(t)S^z_{-\mathbf{k},\beta}(0)\rangle$ for the longitudinal channel, respectively, where $\mathbf{S}_{\mathbf{k},\alpha} = (1/L)\sum_i e^{-i\mathbf{k}\cdot\mathbf{r}_{i,\alpha}}\mathbf{S}_{i,\alpha}$. In what follows, we examine, separately, the traces over the correlation matrices in each channel, $S^{+-}(\mathbf{k},\omega) \coloneqq \sum_\alpha S^{+-}_{\alpha,\alpha}(\mathbf{k},\omega)$, and $S^{zz}(\mathbf{k},\omega) \coloneqq \sum_\alpha S^{zz}_{\alpha,\alpha}(\mathbf{k},\omega)$, respectively, as they contain the full summations over the correlation-matrix eigenvalues of the spectral functions at each fixed momentum transfer.

To calculate the spin spectral functions of the BFG model, we performed QMC simulations using the stochastic series expansion method [35] for system sizes up to $L = 18$. The QMC sampling of this highly frustrated model in the strongly anisotropic QSL regime $J \ll J_z$ was improved by using a decoupling of H in terms of four-site clusters [34,36,37], combined with directed loop updates [38,39]. In order to access ground state properties of the QSL, the temperature T was tuned sufficiently below

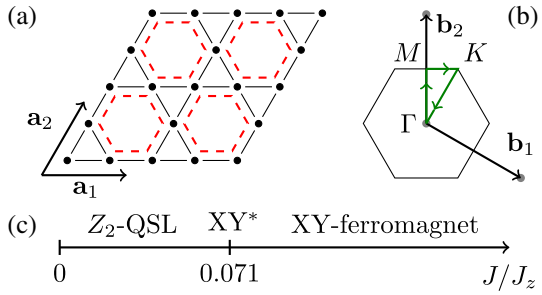

FIG. 1. (a) Kagome lattice with the nearest neighbor exchange (solid lines) and hexagonal cluster (dashed lines) terms of the BFG model. (b) First Brillouin zone (BZ) along with the path $\Gamma \to M \to K \to \Gamma$ (green lines). (c) Ground state phase diagram of the BFG model.

the vison excitation gap, as detailed below. To obtain the DSSF from the QMC simulations, we measured the corresponding transverse imaginary-time displaced spin-spin correlation functions and accessed the longitudinal correlations directly in Matsubara frequency space [40,41], using the stochastic analytic continuation method in the formulation of Ref. [42] to obtain the spectral functions in real frequency space. We performed the analytic continuations independently for the three correlation-matrix eigenvalues for each given momentum $\mathbf{k}$. These are obtained by diagonalizing the 3×3 correlation matrices in the imaginary-time domain, based on the binned QMC time-series data to estimate the corresponding covariances that enter the analytic continuation [42,43]. The spectral functions from the separately continued eigenvalues then yield $S^{+-}(\mathbf{k},\omega)$ and $S^{zz}(\mathbf{k},\omega)$ upon summation.

The benefits of this procedure can be demonstrated by first considering the XY-ferromagnetic limit $J_z = 0$ of the BFG model. In this limit, the system has an XY-ferromagnetic ground state (a superfluid phase in the bosonic formulation of the BFG model), which spontaneously breaks its residual U(1) symmetry. Figure 2 shows $S^{+-}(\mathbf{k},\omega)$ and $S^{zz}(\mathbf{k},\omega)$ along a high-symmetry BZ path [cf. Fig 1(b)], and compares the spectra from the analytic continuation of the direct trace (a), (b) to the summation over the separately continued correlation-matrix eigenvalues (c), (d). Also shown in Fig. 2 are the three magnon branches from linear spin-wave theory (LSWT) for the XY ferromagnet on the kagome lattice, obtained in the Holstein-Primakoff representation from a bosonic Bogoliubov matrix diagonalization [44] in a rotated reference frame [45]. This comparison shows that the

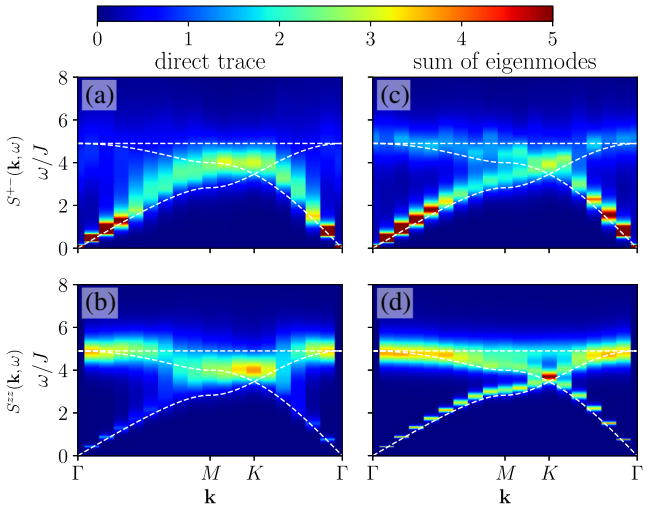

FIG. 2. DSSF $S^{+-}(\mathbf{k},\omega)$ (a), (c) and $S^{zz}(\mathbf{k},\omega)$ (b), (d) of the BFG model for $J_z = 0$ along the BZ path $\Gamma \to M \to K \to \Gamma$, obtained at $T = 0.03J$ on an $L = 18$ lattice. (a) and (b) show results obtained from analytic continuations of the direct correlation-matrix trace, and (c) and (d) show the summed spectra from an eigenvalue decomposition. Dashed lines are magnon branches from LSWT.

eigenvalue decomposition allows for a higher resolution of the distinct modes than the analytic continuation of the direct trace, since the single continuation of the direct trace fails to discern close-by spectral features in frequency space that are due to distinct eigenvalues. In particular, the transverse channel is dominated by the low-energy magnon branch, the Goldstone soft-mode that results from the spontaneous U(1) symmetry breaking. The broad continuum above the lowest magnon branch indicates multimagnon excitations. The Goldstone mode also contributes to $S^{zz}(\mathbf{k},\omega)$ but with a much lower spectral weight that vanishes towards the Γ point. A larger spectral weight is supported by the magnon branches at elevated energies of $\omega \approx 4J$, which the eigenvalue decomposition allows us to separate [cf., e.g., the K point in Fig. 2(d)]. The exactly flat optical magnon mode from LSWT is found to be, at most, weakly dispersive in QMC calculations.

The well-defined low-energy magnon excitations in the XY-ferromagnetic regime contrast strongly to the spin dynamics observed within the QSL regime, which we examine next. The QMC result for $S^{+-}(\mathbf{k},\omega)$ at a value of $J/J_z = 0.06$ is shown in Fig. 3(a) (at even smaller J/J_z, the QMC updates are much less efficient). We observe a broad continuum of gapped excitations, with a minimum gap at the Γ point of about $0.4J_z$. In the strong J_z regime, the low-energy configurations are characterized by states with $S^z_{\hexagon} = 0$ on all hexagons, and a local spin flip creates two neighboring hexagons with $S^z_{\hexagon} = 1$. Because of the transverse exchange $J > 0$, these defects delocalize over the triangular lattice of hexagons, forming two spatially separated spin-1/2 spinon excitations [19]. To quantify the two-spinon contribution to $S^{+-}(\mathbf{k},\omega)$, we use a tight-binding model that treats the spinons as free particles, with a dispersion relation $\epsilon_{\mathbf{k}} = J_z/2 + \epsilon_t(\mathbf{k})$, where $J_z/2$ is the local energy cost of a single spinon, and $\epsilon_t(\mathbf{k}) = -2t[\cos(\mathbf{a}_1\mathbf{k}) + \cos(\mathbf{a}_2\mathbf{k}) + \cos(\mathbf{a}_2\mathbf{k} - \mathbf{a}_1\mathbf{k})]$ the triangular lattice tight-binding dispersion with $t \sim J$ the nearest-neighbor hopping amplitude, fitted to the bandwidth of the QMC continuum. In this approximation, $S^{+-}(\mathbf{k},\omega) \approx [(4\pi)/L^2]\sum_{\mathbf{k}'}\delta(\omega - \epsilon_{\mathbf{k}'} - \epsilon_{\mathbf{k}-\mathbf{k}'})$ is given by the density of two-spinon states, and interaction effects may be accounted for phenomenologically by a Lorentzian δ-function broadening [46,47]. This approximation is shown in Fig. 3(b). Comparisons of the spectra at various fixed momenta are also available [48]. The tight-binding model captures the spectral support of the continuum and the enhanced spectral weight near the BZ corners (K points) at $\omega \approx J_z$. The continuum in $S^{+-}(\mathbf{k},\omega)$ provides a clear signature for deconfined spinons in the QSL phase, in strong contrast to the sharp gapped magnon excitations observed, e.g., in quantum disordered spin-dimer systems or valence bond ordered states [49–51].

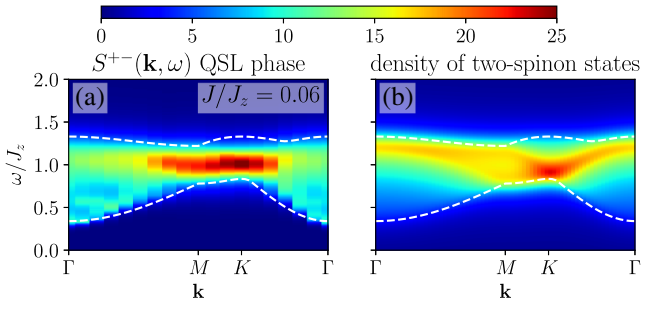

FIG. 3. (a) DSSF $S^{+-}(\mathbf{k},\omega)$ of the BFG model for $J/J_z = 0.06$ within the QSL regime, along the BZ path $\Gamma \to M \to K \to \Gamma$, obtained at $T = 0.002J_z$ on an $L = 18$ lattice. (b) Density of two-spinon states within the tight-binding model with $t = 0.055J_z$, and a Lorentzian δ-function broadening of half-width $2t$. Dashed lines in both panels show the lower and upper threshold of the two-spinon continuum within the tight-binding model.

The two-spinon gap from Fig. 3 corresponds to the activated T dependence of the energy E atop the spin paramagnetic plateau [31] at $T \approx J$, cf. the exponential fit to the data in Fig. 4, which yields $\Delta_s \approx 0.43(2)J_z$. The activated behavior of E at even lower temperatures, $T \ll J$, seen in Fig. 4, instead, arises from the thermal proliferation of vison-pair excitations [31], and from fitting $E(T)$ to an exponential form, we estimate a corresponding two-vison gap of $\Delta_v \approx 0.012(1)J_z$. In the quantum-dimer model limit of the BFG model, for $J/J_z \to 0$, the equal-time vison-vison correlations are given by a string operator of S^z_j operators [19], and correspondingly, two-vison excitations may be probed through the longitudinal channel $S^{zz}(\mathbf{k},\omega)$. The QMC result for $S^{zz}(\mathbf{k},\omega)$ for $J/J_z = 0.06$ is shown in Fig. 5. From the BZ path data in the left panel, we identify an excitation gap at the Γ point in accord with the above estimate. Thus, to obtain the spectral functions, we performed the QMC simulations at a temperature of $T = 0.002J_z$, below the estimated two-vison gap. Based on our data, we cannot discern vison bound states below the continuum. Indications for such bound states were reported for a related quantum dimer model on the triangular lattice [52], for which, also, the single-vison dispersion is available [53], based on which the spectral support of the two-vison continuum could, thus, be constructed and separated from the bound state.

Upon closer inspection, one identifies, in Fig. 5(a), a low-energy structure (at the two-vison gap energy) in

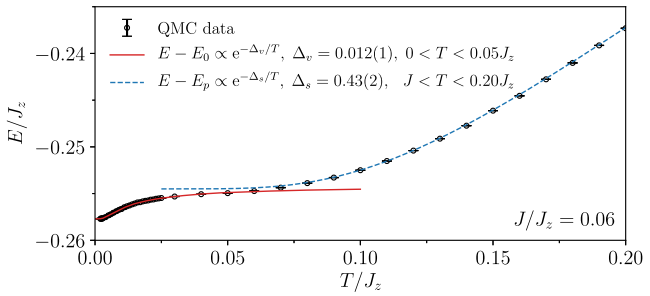

FIG. 4. T dependence of the energy E of the BFG model for $J/J_z = 0.06$, along with exponential fits to activated behavior atop the ground state energy E_0 and the energy plateau $E_p \approx -0.255J_z$ at $T \approx J$ on an $L = 18$ lattice.

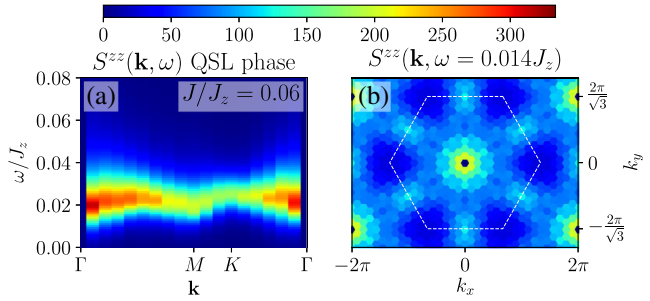

FIG. 5. DSSF $S^{zz}(\mathbf{k},\omega)$ of the BFG model for $J/J_z=0.06$ within the QSL regime at $T=0.002J_z$ on an $L=18$ lattice, (a) along the BZ path $\Gamma\to M\to K\to\Gamma$, and (b) at $\omega=0.014J_z$. The hexagon in (b) denotes the BZ.

$S^{zz}(\mathbf{k},\omega)$ at the M point. This is seen more explicitly in Fig. 5(b), which shows $S^{zz}(\mathbf{k},\omega)$ at a constant energy $\omega=0.014J_z$ (similar cuts at other fixed energies are also available [48]). This repeating structure at the M points of the BZ (at momenta $\pm\mathbf{b}_1/2$, $\pm\mathbf{b}_2/2$, and $\pm(\mathbf{b}_1+\mathbf{b}_2)/2$) is in accord with an enhanced spectral periodicity that is expected in the continuum of the two-vison states, based on the crystal momentum fractionalization of the vison excitations in a Z_2 QSL on the kagome lattice, i.e., anticommuting translation operators T_1 and T_2, $T_1:T_2=-T_2:T_1$, acting on the single vison excitations along the two lattice directions [54–60]. For gapped Z_2 QSL states, such a spectral periodicity was shown to provide a spectroscopic diagnostic of crystal momentum fractionalization of anyon excitations [54,61]. The low-energy spectral weight observed in $S^{zz}(\mathbf{k},\omega)$ at the M points suggests that the QSL state in the considered parameter regime of the BFG model can be driven towards a valence bond solid instability upon adding an appropriate perturbation that couples to valence bond fluctuations at the M points [55,62]. An explicit investigation of such a scenario is provided in Ref. [63].

Finally, we monitor, in Fig. 6, the evolution of the DSSF upon approaching the QSL phase from the XY-ferromagnetic regime. In the transverse channel, we observe (i) a progressive broadening of the lowest magnon branch at high energies upon decreasing J/J_z, along with (ii) a reduced spin-wave velocity (as estimated by the slope of the magnon branch near the Γ point), and (iii) a redistribution of spectral weight to preform the characteristic shape of the spinor-continuum in the QSL phase. In the longitudinal channel, the characteristic energy scale of the predominant optical modes drops rapidly with decreasing J/J_z, an effect that is also qualitatively captured by LSWT. We also observe a strong suppression in the spectral weight of the lowest magnon mode. Upon entering the QSL phase, the other two branches merge, and a gap minimum is formed at the Γ point.

Our results demonstrate the feasibility of probing fractionalization in QSL states from the spin dynamics of microscopic models on relatively large lattices using

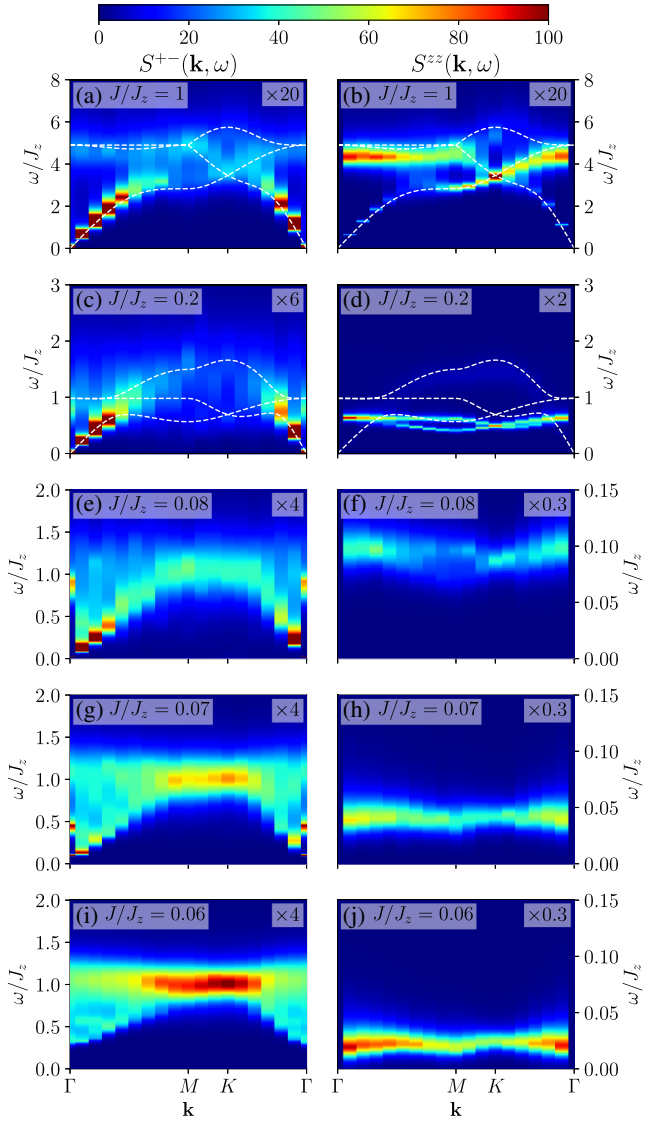

FIG. 6. DSSF $S^{+-}(\mathbf{k},\omega)$ (left panels) and $S^{zz}(\mathbf{k},\omega)$ (right panels) along the BZ path $\Gamma\to M\to K\to\Gamma$ for different ratios J/J_z from QMC simulations at temperatures T near $J/(2L)$ on an $L=18$ lattice. To fit to a common scale, the intensities were multiplied by individual factors, which are provided in the upper right corner of each panel separately. Dashed lines are magnon branches from LSWT.

unbiased numerical methods, such as QMC simulations. It will be intriguing to compare our results to the spin dynamics of other kagome-lattice based QSL states, e.g., with an even Ising gauge structure, which are also accessible to QMC approaches [64]. Furthermore, alternative numerical approaches such as those used in Refs. [65,66] can also probe the spin dynamics of QSL states beyond the realms of unbiased QMC methods.

We thank Z. Y. Meng and Y. Qi for sharing their valuable insight on crystal symmetry fractionalization, and for communicating results from a related study [63]. We also thank F. Hassler, A. M. Läuchli, and F. Pollmann for useful

discussions. Furthermore, we acknowledge support by the Deutsche Forschungsgemeinschaft (DFG) under Grants No. FOR 1807 and No. RTG 1995, and thank the IT Center at RWTH Aachen University and the JSC Jülich for access to computing time through JARA-HPC.

[1] L. Balents, Nature (London) **464**, 199 (2010).
[2] Y. Zhou, K. Kanoda, and T.-K. Ng, Rev. Mod. Phys. **89**, 025003 (2017).
[3] L. Savary and L. Balents, Rep. Prog. Phys. **80**, 016502 (2017).
[4] X.-G. Wen, Rev. Mod. Phys. **89**, 041004 (2017).
[5] S. C. Morampudi, A. M. Turner, F. Pollmann, and F. Wilczek, Phys. Rev. Lett. **118**, 227201 (2017).
[6] M. Fu, T. Imai, T.-H. Han, and Y. S. Lee, Science **350**, 655 (2015).
[7] T.-H. Han, M. R. Norman, J.-J. Wen, J. A. Rodriguez-Rivera, J. S. Helton, C. Broholm, and Y. S. Lee, Phys. Rev. B **94**, 060409 (2016).
[8] Z. Feng, Z. Li, X. Meng, W. Yi, Y. Wei, J. Zhang, Y.-C. Wang, W. Jiang, Z. Liu, S. Li, F. Liu, J. Luo, S. Li, G.-q. Zheng, Z. Y. Meng, J.-W. Mei, and Y. Shi, Chin. Phys. Lett. **34**, 077502 (2017).
[9] X.-G. Wen, Chin. Phys. Lett. **34**, 090101 (2017).
[10] Y. Wei, Z. Feng, W. Lohstroh, C. dela Cruz, W. Yi, Z. F. Ding, J. Zhang, C. Tan, L. Shu, Y.-C. Wang, J. Luo, J.-W. Mei, Z. Y. Meng, Y. Shi, and S. Li, arXiv:1710.02991.
[11] H. C. Jiang, Z. Y. Weng, and D. N. Sheng, Phys. Rev. Lett. **101**, 117203 (2008).
[12] S. Yan, D. A. Huse, and S. R. White, Science **332**, 1173 (2011).
[13] H. Nakano and T. Sakai, J. Phys. Soc. Jpn. **80**, 053704 (2011).
[14] S. Depenbrock, I. P. McCulloch, and U. Schollwöck, Phys. Rev. Lett. **109**, 067201 (2012).
[15] Y. Iqbal, F. Becca, S. Sorella, and D. Poilblanc, Phys. Rev. B **87**, 060405 (2013).
[16] Y. Iqbal, D. Poilblanc, and F. Becca, Phys. Rev. B **91**, 020402(R) (2015).
[17] Y.-C. He, M. P. Zaletel, M. Oshikawa, and F. Pollmann, Phys. Rev. X **7**, 031020 (2017).
[18] H. J. Liao, Z. Y. Xie, J. Chen, Z. Y. Liu, H. D. Xie, R. Z. Huang, B. Normand, and T. Xiang, Phys. Rev. Lett. **118**, 137202 (2017).
[19] L. Balents, M. P. A. Fisher, and S. M. Girvin, Phys. Rev. B **65**, 224412 (2002).
[20] X.-G. Wen, Phys. Rev. B **44**, 2664 (1991).
[21] X.-G. Wen, Int. J. Mod. Phys. B **05**, 1641 (1991).
[22] F. J. Wegner, J. Math. Phys. (N.Y.) **12**, 2259 (1971).
[23] E. Fradkin and L. Susskind, Phys. Rev. D **17**, 2637 (1978).
[24] J. B. Kogut, Rev. Mod. Phys. **51**, 659 (1979).
[25] T. Senthil and M. P. A. Fisher, Phys. Rev. B **62**, 7850 (2000).
[26] T. Senthil and M. P. A. Fisher, Phys. Rev. Lett. **86**, 292 (2001).
[27] R. Moessner, S. L. Sondhi, and E. Fradkin, Phys. Rev. B **65**, 024504 (2001).
[28] M. Punk, D. Chowdhury, and S. Sachdev, Nat. Phys. **10**, 289 (2014).
[29] D. N. Sheng and L. Balents, Phys. Rev. Lett. **94**, 146805 (2005).
[30] S. V. Isakov, Y. B. Kim, and A. Paramekanti, Phys. Rev. Lett. **97**, 207204 (2006).
[31] S. V. Isakov, A. Paramekanti, and Y. B. Kim, Phys. Rev. B **76**, 224431 (2007).
[32] S. V. Isakov, M. B. Hastings, and R. G. Melko, Nat. Phys. **7**, 772 (2011).
[33] S. V. Isakov, R. G. Melko, and M. B. Hastings, Science **335**, 193 (2012).
[34] Y.-C. Wang, C. Fang, M. Cheng, Y. Qi, and Z. Y. Meng, arXiv:1701.01552.
[35] A. W. Sandvik, Phys. Rev. B **59**, R14157 (1999).
[36] K. Louis and C. Gros, Phys. Rev. B **70**, 100410(R) (2004).
[37] R. G. Melko, J. Phys. Condens. Matter **19**, 145203 (2007).
[38] O. F. Syljuasen and A. W. Sandvik, Phys. Rev. E **66**, 046701 (2002).
[39] F. Alet, S. Wessel, and M. Troyer, Phys. Rev. E **71**, 036706 (2005).
[40] F. Michel and H. G. Evertz, arXiv:0705.0799.
[41] F. Michel, Ph.D. Thesis, University of Graz, 2007.
[42] K. S. D. Beach, arXiv:cond-mat/0403055.
[43] M. Jarrell and J. E. Gubernatis, Phys. Rep. **269**, 133 (1996).
[44] J. Avery, *Creation and Annihilation Operators* (McGraw-Hill, New York, 1976), Appendix 1 and references therein.
[45] V. A. Stephanovich and M. E. Zhitomirsky, Europhys. Lett. **95**, 17007 (2011).
[46] S. Kourtis and C. Castelnovo, Phys. Rev. B **94**, 104401 (2016).
[47] C.-J. Huang, Y. Deng, Y. Wan, and Z. Y. Meng, Phys. Rev. Lett. **120**, 167202 (2018).
[48] See Supplemental Material at http://link.aps.org/supplemental/10.1103/PhysRevLett.121.077202 for (i) the transverse spectral functions at various fixed momenta within the QSL regime, and (ii) the dynamical spin structure factors at fixed energies within the QSL regime.
[49] M. Lohöfer, T. Coletta, D. G. Joshi, F. F. Assaad, M. Vojta, S. Wessel, and F. Mila, Phys. Rev. B **92**, 245137 (2015).
[50] M. Lohöfer and S. Wessel, Phys. Rev. Lett. **118**, 147206 (2017).
[51] N. Ma, G.-Y. Sun, Y.-Z. Yuo, C. Xu, A. Vishwanath, A. W. Sandvik, and Z. Y. Meng, arXiv:1803.01180.
[52] A. M. Läuchli, S. Capponi, and F. F. Assaad, J. Stat. Mech. (2008) P01010.
[53] D. A. Ivanov, Phys. Rev. B **70**, 094430 (2004).
[54] X.-G. Wen, Phys. Rev. B **65**, 165113 (2002).
[55] Y. Huh, M. Punk, and S. Sachdev, Phys. Rev. B **84**, 094419 (2011).
[56] A. M. Essin and M. Hermele, Phys. Rev. B **87**, 104406 (2013).
[57] Y. Qi and L. Fu, Phys. Rev. B **91**, 100401(R) (2015).
[58] Y. Qi, M. Cheng, and C. Fang, arXiv:1509.02927.
[59] Y. Qi and M. Cheng, Phys. Rev. B **97**, 115138 (2018).
[60] M. Cheng, M. Zaletel, M. Barkeshli, A. Vishwanath, and P. Bonderson, Phys. Rev. X **6**, 041068 (2016).
[61] A. M. Essin and M. Hermele, Phys. Rev. B **90**, 121102(R) (2014).
[62] C. Xu and S. Sachdev, Phys. Rev. B **79**, 064405 (2009).

[63] G. Y. Sun, Y.-C. Wang, C. Fang, Y. Qi, M. Cheng, and Z. Y. Meng, preceding Letter Phys. Rev. Lett. **121**, 077201 (2018).
[64] Y.-C. Wang, X. F. Zhang, F. Pollmann, M. Cheng, and Z. Y. Meng, arXiv:1711.03679 [Phys. Rev. Lett. (to be published)].
[65] M. Gohlke, R. Verresen, R. Moessner, and F. Pollmann, Phys. Rev. Lett. **119**, 157203 (2017).
[66] S. M. Winter, K. Reidl, P. A. Maksimov, A. L. Chernyshev, A. Honecker, and R. Valenti, Nat. Commun. **8**, 1152 (2017).